ELSEVIER

NeuroImage

www.elsevier.com/locate/ynimg
NeuroImage 35 (2007) 1113 – 1124

Transcranial direct current stimulation: A computer-based human model study

Tim Wagner,[a,b,c,*] Felipe Fregni,[a] Shirley Fecteau,[a] Alan Grodzinsky,[b,d] Markus Zahn,[b] and Alvaro Pascual-Leone[a,*]

[a]*Center for Non-invasive Brain Stimulation, Beth Israel Deaconess Medical Center, Harvard Medical School, Boston, MA 02115, USA*
[b]*Department of Electrical Engineering and Computer Science, Massachusetts Institute of Technology, Cambridge, MA 02139, USA*
[c]*Division of Health Sciences and Technology, Harvard Medical School/Massachusetts Institute of Technology, Boston, MA 02114, USA*
[d]*Center for Biomedical Engineering, Massachusetts Institute of Technology, Cambridge, MA 02115, USA*

Received 1 June 2006; revised 9 November 2006; accepted 3 January 2007
Available online 4 February 2007

Objectives: **Interest in transcranial direct current stimulation (tDCS) in clinical practice has been growing, however, the knowledge about its efficacy and mechanisms of action remains limited. This paper presents a realistic magnetic resonance imaging (MRI)-derived finite element model of currents applied to the human brain during tDCS.**
Experimental design: **Current density distributions were analyzed in a healthy human head model with varied electrode montages. For each configuration, we calculated the cortical current density distributions. Analogous studies were completed for three pathological models of cortical infarcts.**
Principal observations: **The current density magnitude maxima injected in the cortex by 1 mA tDCS ranged from 0.77 to 2.00 mA/cm^2. The pathological models revealed that cortical strokes, relative to the non-pathological solutions, can elevate current density maxima and alter their location.**
Conclusions: **These results may guide optimized tDCS for application in normal subjects and patients with focal brain lesions.**

Keywords: Finite element model; Stroke; Neuro-model; Brain polarization; MRI; Brain stimulation

Introduction

Transcranial direct current stimulation (tDCS) is a noninvasive brain stimulation technique that utilizes low amplitude direct currents applied via scalp electrodes to inject currents in the brain and modulate the level of cortical excitability (Nitsche and Paulus, 2000). Although forms of DC stimulation have been used since the inception of modern electrophysiology (Aldini, 1804), there has been a recent upsurge in interest in tDCS as a tool for neuroscience research (Nitsche and Paulus, 2001; Antal et al., 2003) and for the treatment and assessment of various neurological and psychiatric disorders (Fregni et al., 2005a, 2006a,b; Nitsche, 2002). tDCS saw a similar increase in interest in the 1960s (Bindman et al., 1964; Purpura and McMurtry, 1965), but was largely abandoned due to inconsistent results in human trials (Bindman et al., 1964; Sheffield and Mowbray, 1968; Hall et al., 1970; Lolas, 1976). As in the 1960s, there are still many fundamental unresolved questions concerning the stimulating current densities injected by tDCS, including questions as to whether currents of sufficient magnitude even reach the cortex to influence neural activity (Barker, 1994; Nathan et al., 1993); how differences in the electrode configurations influence the stimulating currents (Nitsche and Paulus, 2000, 2001; Priori, 2003); and how various differences in brain anatomy induced by neurological disorders, such as stroke, influence the stimulating currents (Fregni et al., 2005a). Thus, although behavioral (Nitsche et al., 2002) and imaging studies (Nitsche et al., 2004b) suggest the 'brain effects' of tDCS, little has been done to quantify the current densities injected during stimulation, to compare them to published current density magnitudes necessary for neural stimulation, or to analyze how different stimulation parameters can influence the stimulating currents.

Therefore, we analyzed several magnetic resonance imaging (MRI)-derived finite element models (FEM) of electrical current applied to the human cortex during tDCS to: (i) determine cortical current density distributions from various electrode montages used in clinical investigations; (ii) determine the role that tissue heterogeneities and anatomical variations play on the final current

* Corresponding authors. Harvard Center for Non-invasive Brain Stimulation-330 Brookline Ave #KS452-Boston, MA 02115, USA. Fax: +1 617 975 5322.
E-mail addresses: twagner@mit.edu (T. Wagner), apleone@bidmc.harvard.edu (A. Pascual-Leone).
Available online on ScienceDirect (www.sciencedirect.com).

1053-8119/$ - see front matter © 2007 Elsevier Inc. All rights reserved.
doi:10.1016/j.neuroimage.2007.01.027

density distributions; (iii) explore the effects of anatomical–pathological alterations that occur in stroke on the stimulating cortical current densities.

Material and methods

MRI guided finite element head model

Multiple MRI-derived finite element head models using different electrodes montages were constructed. An initial sinusoidal steady-state FEM was developed using the Ansoft 3D Field Simulator software package with the conduction solver (Ansoft, 2005b). The FEM method allows one to break down structures into smaller geometric units, that comprise the FEM mesh, and assign distinct electrical properties to the individual elements, based on the corresponding tissue characteristics, on which discrete approximations of the governing physical equations can more easily and fully be solved. The FEM geometrical mesh structure was constructed from an MRI guided three-dimensional Computer Aided Design (CAD) rendering of the human head. The MRI images were used to segment the modeled tissues in the FEM space, guiding the mesh generation based on the MRI-derived tissue boundaries, the process of which is detailed in Wagner et al. (2004). We refer to this as the healthy head model (see Fig. 1A; note that the coordinate system used in this paper is defined in the figure). This model was generated to include the skin, skull, cerebrospinal fluid (CSF), gray matter, and white matter. The tissue conductivities of the base healthy head model were assigned the mean value from multiple references: skin: 0.465 S/m; bone: 0.010 S/m; CSF: 1.654 S/m; gray matter: 0.276 S/m; white matter: 0.126 S/m (Akhtari et al., 2002; Burger and Van Milaan, 1943; Crille et al., 1922; De Mercato and Garcia Sanchez, 1992; Freygang and Landau, 1955; Gabriel and Gabriel, 1996; Geddes, 1987; Hasted, 1973; Lepeschkin, 1951; Oswald, 1937; Radvan-Ziemnowicz et al., 1964; Ranck, 1963).

Field solver

The Ansoft FEM solver was set to solve for the current densities in terms of the electric potential (ϕ), by solving the equation: $\nabla\cdot(\sigma_i\nabla\phi)=0$, where σ_i is the conductivity of the tissue (Ansoft). The solution method followed an adaptive iterative process with convergence limits determined by the energy error in the system (for more details, see Ansoft, 2005a; Bogdan and Zhou, 2004; Wagner et al., 2004). The criterion for model convergence was defined as an energy error below 1.0%.

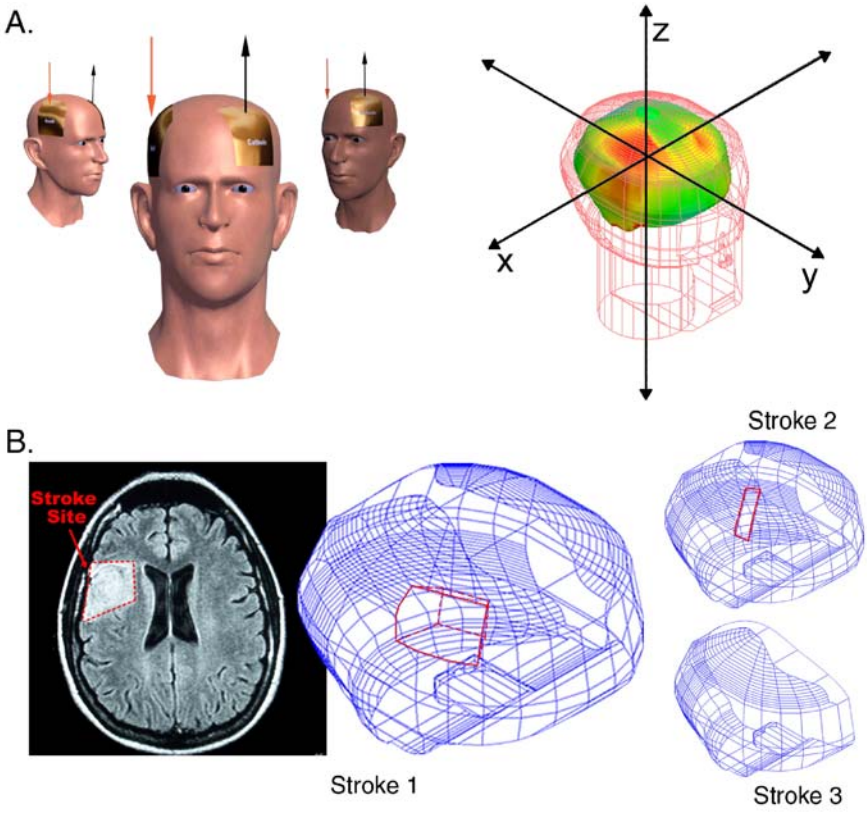

Fig. 1. Model system. (A) Here is an example of the healthy head model with the anode at the right primary motor cortex (M1)–cathode on the left supra-orbital electrode montage (Montage 1A). In the right most part of the figure the coordinate system is defined in the image that shows the outline of FEM mesh of the skin and the gray matter surface current density solution for this solution. (B) The gray matter FEM mesh outline for Stroke 1 and a slice from the MRI used to develop the model are shown in the left part of the figure. The gray matter mesh outlines for Strokes 2 and 3 are shown on the right. Stroke 1 had an approximate volume of 18.5 cm3 with a maximum 2.5 cm inferior to superior length along the cortical face, a maximum anterior to posterior length of 3.5 cm along the cortical face, and a maximum depth of 2.8 cm measured from the cortical face. Stroke 2 had an approximate volume of 5.3 cm^3 with a maximum inferior to superior length of 4 mm along the cortical face, a maximum anterior to posterior length of 4 mm along the cortical face, and a maximum depth of 4 mm measured from the cortical face. Stroke 3 had a 350 cm^3 volume and was designed by removing the cortical mantle of the left hemisphere from the model.

Model specification

The following specific electrode montages and head models were implemented to explore the effects of electrodes, tissues, and pathologies on tDCS stimulating currents.

Electrode size/current density

The effects of varying the area of the surface electrodes were analyzed. Rectangular electrode pairs of 7×7 cm^2, 7×5 cm^2, 5×5 cm^2, and 1×1 cm^2 were placed on the scalp overlaying the right M1 (anode) and the contralateral supra-orbital region (cathode). We chose these electrode sizes as several tDCS studies have been conducted in humans using 5×7 cm^2 electrodes (Fregni et al., 2005a, 2006a,b; Nitsche et al., 2004a; Nitsche and Paulus, 2000, 2001) and 5×5 cm^2 electrodes (Hummel et al., 2005; Iyer et al., 2005). We then chose extreme boundaries (7×7 and 1×1 cm^2 electrodes) to further explore the effects of contact area. The electrodes were modeled as planar current boundaries on the scalp surface, where 1 mA total current was applied at the anode location. The electrode placement schemes and average electrode current density magnitudes are included in Table 1.

The current density distributions were analyzed for each electrode montage. The magnitude and location of the maximum cortical current density were evaluated for each electrode montage and individually for each electrode (i.e., the maximum cortical current density proximal to the anode was not always equivalent to the maximum near the cathode). Additionally, the surface area on the cortex where the current density was greater than 90% of its maximum value, referred to as the maximum cortical current surface area, was calculated for each electrode. Finally, the variation in the current density across the different tissues was evaluated. To quantify the shunting effect, we divided the average maximum skin current density by the maximum cortical current density, where the average maximum skin current density was defined as the current density magnitude on the skin for which at least 0.5 cm^2 in area was covered and which was not confined to the electrode boundary edge effects (Kim et al., 1984; Lindemanns et al., 1975; Nathan et al., 1993). The exact current density analysis was also completed for reversed polarity electrode montages, where the anode was made the cathode and vice versa.

Electrode placement

The effects of varying the position of the surface electrodes on the tDCS current densities were analyzed. The following electrode placements were analyzed: (1) anode over the right M1–cathode over the left supra-orbital region; (2) anode over the right M1–cathode over the left M1; (3) anode over the primary visual cortex (V1)–cathode over the vertex; (4) anode over V1–cathode over the left supra-orbital region; (5) anode over the left dorsolateral prefrontal cortex (DLPFC)–cathode over the right supra-orbital region; and (6) anode over the right DLPFC–cathode over the left DLPFC. In these cases the electrodes were 5×7 cm^2 with a total applied current of 1 mA. Solutions were also obtained for a 5×7 cm^2 anode above the right M1 and a 5×7 cm^2 cathode electrode on the contralateral lower neck. For each solution, the current densities were analyzed as detailed above (see Fig. 1A for an example of the anode over the right M1–cathode over the left supra-orbital region electrode montage; the full list of montages is tabulated in Table 1).

Table 1
Electrode montages

Montage	Electrode	Size	Placement	Total current	Current density
1	Anode	7×7	Right M1	1	2.0
	Cathode	7×7	Left supra-orbital		−2.0
2	Anode	5×7	Right M1	1	2.9
	Cathode	5×7	Left supra-orbital		−2.9
3	Anode	5×5	Right M1	1	4.0
	Cathode	5×5	Left supra-orbital		−4.0
4	Anode	1×1	Right M1	1	100.0
	Cathode	1×1	Left supra-orbital		−100.0
7	Anode	5×7	Right M1	1	2.9
	Cathode	5×7	Left M1		−2.9
8	Anode	5×7	Right DLPFC	1	2.9
	Cathode	5×7	Left supra-orbital		−2.9
9	Anode	5×7	V1	1	2.9
	Cathode	5×7	Left supra-orbital		−2.9
10	Anode	5×7	Right M1	1	2.9
	Cathode	5×7	Left lower neck		−2.9
11	Anode	5×7	Right DLPFC	1	2.9
	Cathode	5×7	Left DLPFC		−2.9
12	Anode	5×7	V1	1	2.9
	Cathode	5×7	Vertex		−2.9
Strokes 1–3	Anode	5×7	Right M1	1	2.9
	Cathode	5×7	Left supra-orbital		−2.9
Stroke 1B	Anode	5×7	Right M1	1	2.9
	Cathode	5×7	Left M1		−2.9

Electrode Montages: The Montage name is provided in the left column, anode and cathode distinction in the second column, electrode area in square centimeters in the third column, electrode placement in the fourth column, the total current in the closed loop circuit which drives stimulation (in mA), and the average current density at each contact point in the sixth column (in mA/cm^2). The average electrode current density magnitudes are reported as the total current in the electrode divided by the total electrode area.

Stroke models

We implemented three stroke models of various geometries to explore the effects of anatomical perturbations on the current injected by tDCS. To represent the infarction site in the FEM geometry, CSF was used to replace the damaged tissue as shown by both imaging and histopathology studies in the post acute stage (Jacobs et al., 2001; Soltanian-Zadeh et al., 2003). As there have been no studies reporting the conductivity alterations at the gray matter white matter interface proximal to the infarction region (Foster and Schwan, 1996), the tissue was considered continuous cerebral tissue (conductivity = 0.276 S/m). Strokes 1 and 2 were located in the right frontal lobe and modeled to represent infarctions of the superior branches of the right middle cerebral artery. Stroke 1 had an approximate volume of 18.5 cm^3 with a maximum 2.5 cm inferior to superior length along the cortical face, a maximum anterior to posterior length of 3.5 cm along the cortical face, and a maximum depth of 2.8 cm measured from the cortical face. Stroke 2 had an approximate volume of 2.6 cm^3 with a maximum inferior to superior length of 40 mm along the cortical face, a maximum anterior to posterior length of 20 mm along the cortical face, and a maximum depth of 4 mm measured from the cortical face. Finally, Stroke 3 represented a large stroke due to a left MCA occlusion with poor collateral perfusion due to atherosclerotic vascular disease; its size was approximately 350 cm^3 and it was designed by removing the cortical mantle of the left hemisphere from the model. Strokes 1–3 are displayed in Fig. 1B.

In these stroke models, solutions were obtained for electrode pairs (area 5×7 cm^2, 1 mA) placed over the right M1 (anode)–contralateral supra-orbital region (cathode). We also studied Stroke 1 with the anode over the right M1–cathode over the left M1 (5×7 cm^2, 1 mA) electrode montage (we refer to this as Stroke 1B). For each solution, the current densities were analyzed and compared to the analogous healthy head models.

Results

Same electrode montage with variable electrode sizes

For the varied size electrode montages in the healthy head model with the anode placed above M1 and the cathode above the contralateral supra-orbital region, the maximum cortical current densities ranged from 0.81 to 1.41 mA/cm^2. As a function of the injected current density on the scalp surface, the largest cortical

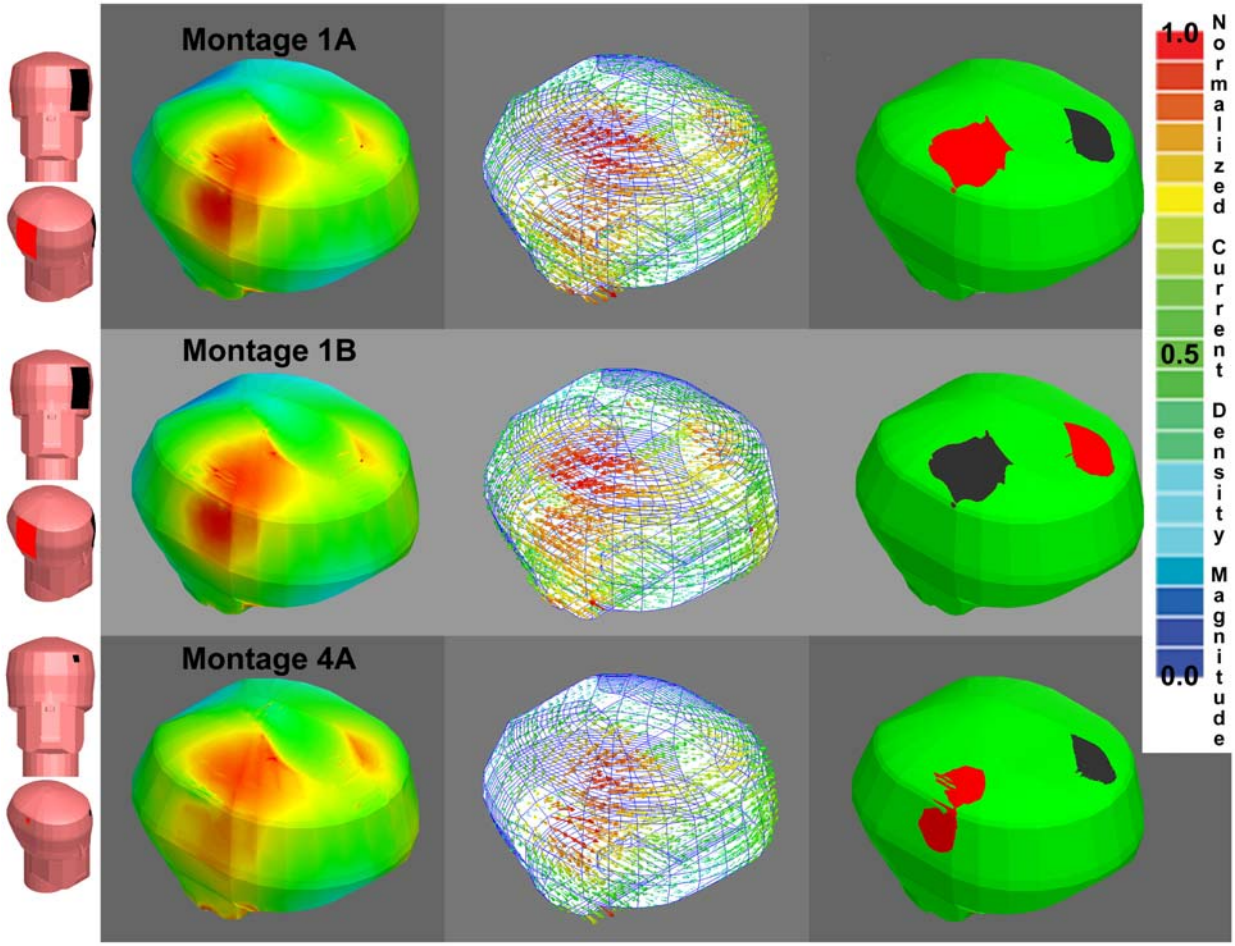

Fig. 2. Cortical current densities for Montages 2, 2 with the polarity reversed, and 4 in the healthy head model. The first column displays the cortical current density along the surface of the gray matter for each solution. The second column displays the current vector distributions on the cortical surface. Note that the scale for the first two columns is normalized to the maximum cortical current density for each separate solution. The third column displays the maximum cortical current surface areas for the anode (in red) and the cathode (in black). On the left edge of the figure, the skin meshes are shown with outlines of the electrodes (anode (red) and cathode (black)) for each stimulation condition.

Table 2
Current density magnitudes

Montage	Electrode	MCCD	Location		Area	AMSCD	Shunting
1	Anode (7×7)	0.91	(36.2, 17.75, 32.89)	Motor strip	13.7	7.90	8.68
	Cathode (7×7)	0.81	(−16.7, 54.7, 32.1)	Frontal lobe	3.31	9.36	11.56
2	Anode (5×7)	0.98	(47.1, 27.5, 26.9)	Motor strip	11.25	9.80	10.00
	Cathode (5×7)	0.84	(−14.5, 50.8, 27.3)	Frontal lobe	3.06	12.20	14.52
3	Anode (5×5)	1.03	(38.2, 26.0, 29.7)	Motor strip	7.78	11.20	10.87
	Cathode (5×5)	0.88	(−16, 55, 31.3)	Frontal lobe	2.85	12.80	14.54
4	Anode (1×1)	1.44	(53.5, 22.75, 11.3)	Motor strip	3.3	52.0	36.11
	Cathode (1×1)	1.12	(−14.4, 51.48, 31.6)	Frontal lobe	1.65	97.0	86.61
7	Anode (5×7)	1.04	(38.6, 0.5, 31.1)	Motor (superior)	16.8	9.20	8.85
	Cathode (5×7)	1.04	(−38.5, 0.4, 31.1)	Motor (superior)	16.8	9.20	8.85
8	Anode (5×7)	0.93	(26.3, 51.9, 28.9)	Frontal lobe	6.4	10.70	11.51
	Cathode (5×7)	0.86	(−17.1, 56.6, 32.2)	Frontal lobe	5.84	11.70	13.60
9	Anode (5×7)	0.96	(−1.52, −63.2, −13.3)	V1	18.7	8.70	9.0625
	Cathode (5×7)	0.79	(−30.8, 42.9, 32)	Frontal lobe	16.2	11.10	14.05
10	Anode (5×7)	0.85	(55.8, 16.6, −8.9)	Motor (inferior)	4.90	9.0	10.6
	Cathode (5×7)			None		13.1	
11	Anode (5×7)	0.77	(18.0, 62.7, 27.97)	Frontal lobe	Merged	13.30	17.27
	Cathode (5×7)	0.77	(−18.0, 62.7, 28.0)	Frontal lobe	Merged	13.30	17.27
12	Anode (5×7)	2.0	(0, −20.1, 37.8)	Merged above v1	3.25	11.70	5.85
	Cathode (5×7)	2.0				14.30	7.15

Current density magnitudes: The first column reports the electrode Montage, the second problem the specific electrode (and size in cm^2), the third reports the maximum cortical current density (MCCD) in mA/cm^2, the fourth and fifth report the location of the MCCD, the sixth reports the area of the maximum cortical current density, the seventh reports the average maximum skin current density, and the final reports the extent of shunting for each electrode Montage.

current density was seen for the 7×7 cm^2 electrode scheme. As expected, when the polarity of the electrodes was reversed the current reversed by 180° (see Fig. 2). The locations of cortical maxima were always within the region of the electrode, essentially lying along the superior portion of the motor strip (see Fig. 2). The results are tabulated in Table 2.

The maximum cortical current surface areas ranged from 3.24 to 13.7 cm^2 for the electrode over the M1 and from 1.48 to 3.36 cm^2 for the electrode over the contralateral supra-orbital (see Fig. 2). The areas were always greater when the electrode was placed over M1 than over the contralateral supra-orbital region. In general, when the electrode was placed over M1, the maximum

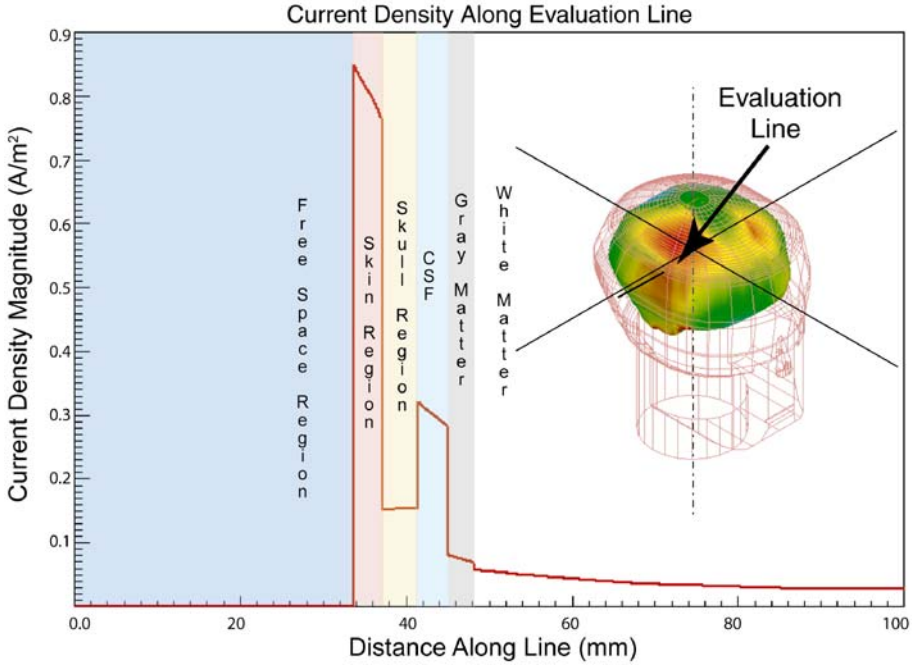

Fig. 3. Current density behavior through tissues. Current density magnitude evaluated along an evaluation line in the healthy head model for Montage 1A. The inset shows mesh model with the current density magnitude plotted on the surface of the cortex with the evaluation line shown intersecting the tissues—the current density magnitudes displayed in the primary graph were calculated along this line. Note that the current density magnitude varies with the conductivity of the tissues.

cortical current surface areas increased with increasing electrode surface area. However, when the electrode was placed above the contralateral supra-orbital region, the maximum cortical current surface areas did not vary much between the 7×7 cm^2, 5×7 cm^2, and 5×5 cm^2 electrode schemes (slightly decreasing with decreasing surface area), and only decreased by a factor of approximately two for the 1×1 cm^2 electrodes. These results are tabulated in Table 2.

The current density vector distribution followed largely the same course and orientation for all of the varied electrode sizes (with differences in the relative magnitudes). The greatest difference was observed between the 7×7 and 1×1 cm^2 electrode schemes, where the larger electrode surface area corresponded to a less focal distribution. For all of the electrode schemes, the largest currents were oriented along the superior part of the right motor strip across the hemispheres and through the left superior medial frontal lobe (see Fig. 2 for a graphical representation of the distributions).

The current density magnitudes varied substantially throughout the tissues, and stair step jumps in the current density occurred at each tissue boundary (see Fig. 3). The largest current density magnitude was located near the edge of the electrodes on the skin surface. These largest current density values on the skin were restricted to small areas, were not reflective of the average current densities magnitudes on the skin or of the shunting effects along the skin (see Fig. 4), and have been explored in depth by other researchers (Kim et al., 1984; Nathan et al., 1993; Lindemanns et al., 1975). The average maximum skin current densities increased with decreasing electrode surface area. To quantify the shunting effect, we divided the average maximum skin current density by the maximum cortical current density. There were drastically greater levels of shunting for the 1×1 cm^2 electrodes than for the larger electrode schemes. These shunting levels ranged from 36.11–86.61 for the 1×1 cm^2 montages to 8.7–14.5 for the larger electrodes. These values are presented in Table 2.

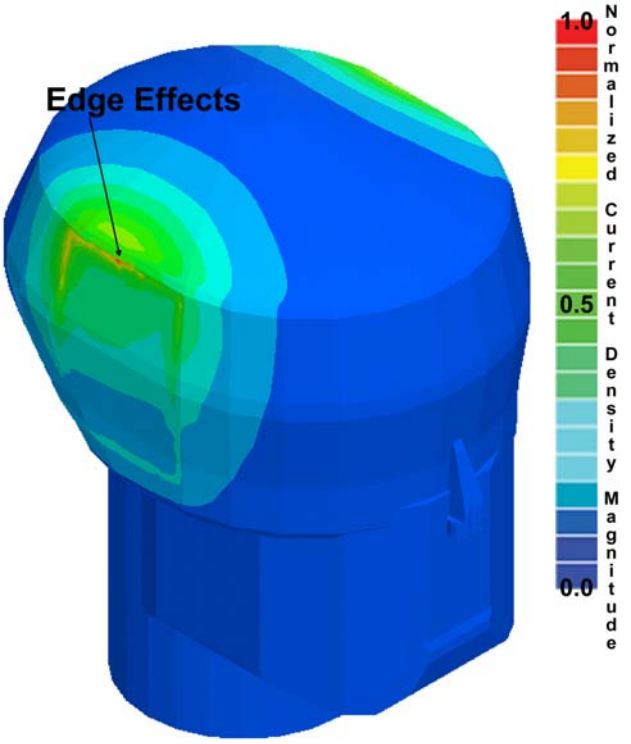

Fig. 4. Skin surface current density for electrode Montage 7. Note the drastic edge effect at the electrode boundary location, current density of 2.06 A/m2, compared to the average maximum skin current density of 0.92 A/m2.

Same electrode size and variable electrode positions

For the fixed size/varied position electrode montages, the maximum cortical current densities ranged from 0.77 to 2.00 mA/cm^2 at the anode and at the cathode. The locations of cortical maxima were within the tissue underlying the electrodes. These results are tabulated in Table 2. The maximum cortical current surface areas ranged from 3.25 to 18.7 cm^2 at the anode and from 3.06 to 16.8 cm^2 at the cathode. For the 'anode over the right DLPFC–cathode over the left DLPFC' and for the 'anode over V1–cathode over vertex' electrode montages, the areas of maximal cortical current were merged at the electrode sites in the sense that there was no clear demarcation of the maximum cortical current surface density under the anode and the cathode (see Fig. 5). The current density vector distributions varied considerably between the various electrode schemes and are graphically displayed in Fig. 5.

Stroke model

The current density distributions were altered in the three stroke models compared to the healthy head model with the same electrode scheme ('anode over right M1–cathode over supra-orbital region', area 5×7 cm^2, 1 mA). The current density maxima were slightly larger and located at different locations in these solutions compared to the healthy head model (see Table 3). The maxima were found along the boundary of the infarction in the Stroke 1 and Stroke 2 models, and more lateral and inferior in the Stroke 3 model. For the Stroke 1 and Stroke 2 models the maximum cortical current density areas were more focal than in the non-stroke case. For Stroke 1B, the current density behavior in the region of the stroke was similar to that of Stroke 1, and was similar in behavior around the cathode to that Montage 7. For all of the solutions, the current density vector orientations were altered at the infarction border (see Fig. 6). Additionally, the current density distributions were nearly unchanged on the surface of the skin, but substantially different in both the CSF and cerebral tissue in the infarctions as compared with the normal condition (see Table 3).

Discussion

This study investigated the behavior of the currents injected in the human brain by tDCS. Our models were based on a finite element electromagnetic solver integrated with MRI-derived head models. The analysis focused on injected cortical current densities exploring the effects of varied electrode montages and varied electrode sizes, shunting in the tissues, and the effects of stroke on the stimulating current density distributions.

Does "stimulation" occur with tDCS?

In the classic sense of the term, stimulation implies the active initiation of an action potential via an outside stimulus. The current density magnitudes that we report are far lower than action potential thresholds from controlled electrical stimulation experiments of cortical neurons (0.79 to 2.00 mA/cm^2 compared to 220 to 2750 mA/cm^2 (Tehovnik, 1996)). Given such drastic differences, it is not surprising that some researchers have

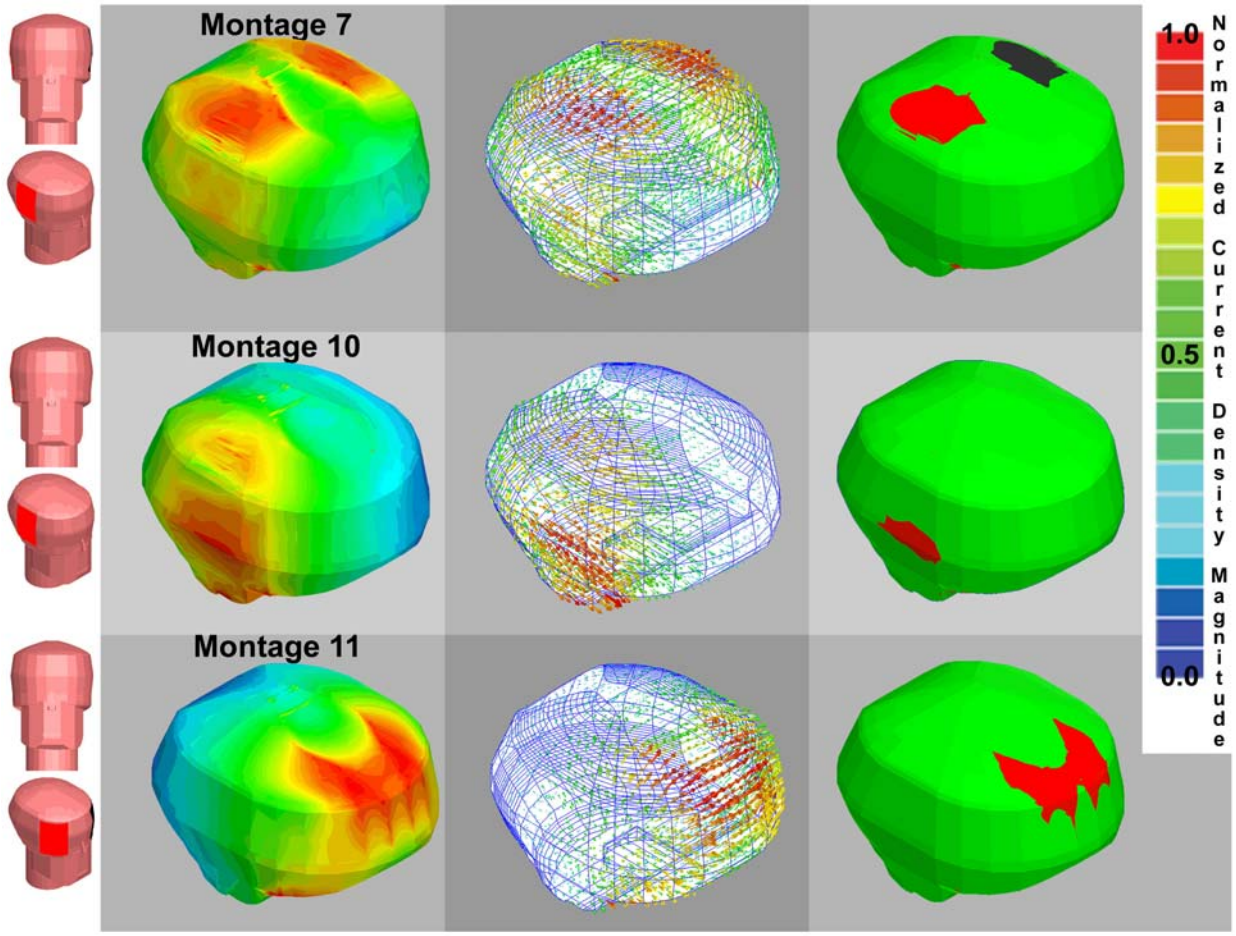

Fig. 5. Cortical current densities for Montages 7, 10, and 11 in the healthy head model. The layout is as explained in Fig. 2.

questioned the therapeutic effects of tDCS (Arfai et al., 1970). However, it is possible that tDCS does not actively 'stimulate' the cortex in the classic sense of the term, but rather it 'modulates' the cortical excitability. In the early 1960s, DC currents as low as 2.5 mA/cm^2, applied to the exposed pia via surface electrodes, were shown to influence spontaneous activity and characteristics of the evoked response from cortical neurons for hours after just minutes of stimulation (Bindman et al., 1964). Note that in these studies the stimulus was applied through the pia, and given the expected current spread, the current density magnitudes at the cortical neurons would be expected to be lower or similar to what has been shown by our models. Thus, our models provide evidence that tDCS injects an electric current into the cortex that has the necessary magnitude to cause biological effects (Bindman et al., 1964; Purpura and McMurtry, 1965) even though it is unlikely to directly induce action potentials, as the injected current densities are below the threshold of cortical neurons (see above and Tehovnik, 1996). The alterations in cortical excitability are thought to be brought about by hyperpolarizing or depolarizing shifts in the resting membrane

Table 3
Current density magnitudes for the stroke models

Montage	Electrode	MCCD	Location		Area	AMSCD	Shunting
Stroke 1	Anode	1.27	(56, 18.2, 17.5)	Stroke border	1.1	9.7	7.64
	Cathode	0.81	(−29.8, 77.6, 14.5)	Frontal lobe	5.12	13	16.05
Stroke 2	Anode	1.16	(53.4, 25.8, 27.3)	Stroke border	1.6	10	8.62
	Cathode	0.80	(−29.63, 68.9, 11.7)	Frontal lobe	4.3	12.6	15.75
Stroke 3	Anode	1.10	(56, 27.83, 1.81)	Motor (lower)	3.17	10.6	9.64
	Cathode	Cortex removed under cathode			12.3		
Stroke 1B	Anode	1.31	(56.2, 18.0, 16.3)	Stroke border	1.2	9.70	7.40
	Cathode	1.06			16.4	9.30	8.77

Current density magnitudes for the stroke models: The first column reports the electrode scheme, the second reports the specific electrode, the third reports the maximum cortical current density (MCCD) in mA/cm^2, the fourth and fifth report the location of the MCCD, the sixth reports the area of the maximum cortical current density, the seventh reports the average maximum skin current density, and the final reports the extent of shunting for each electrode scheme.

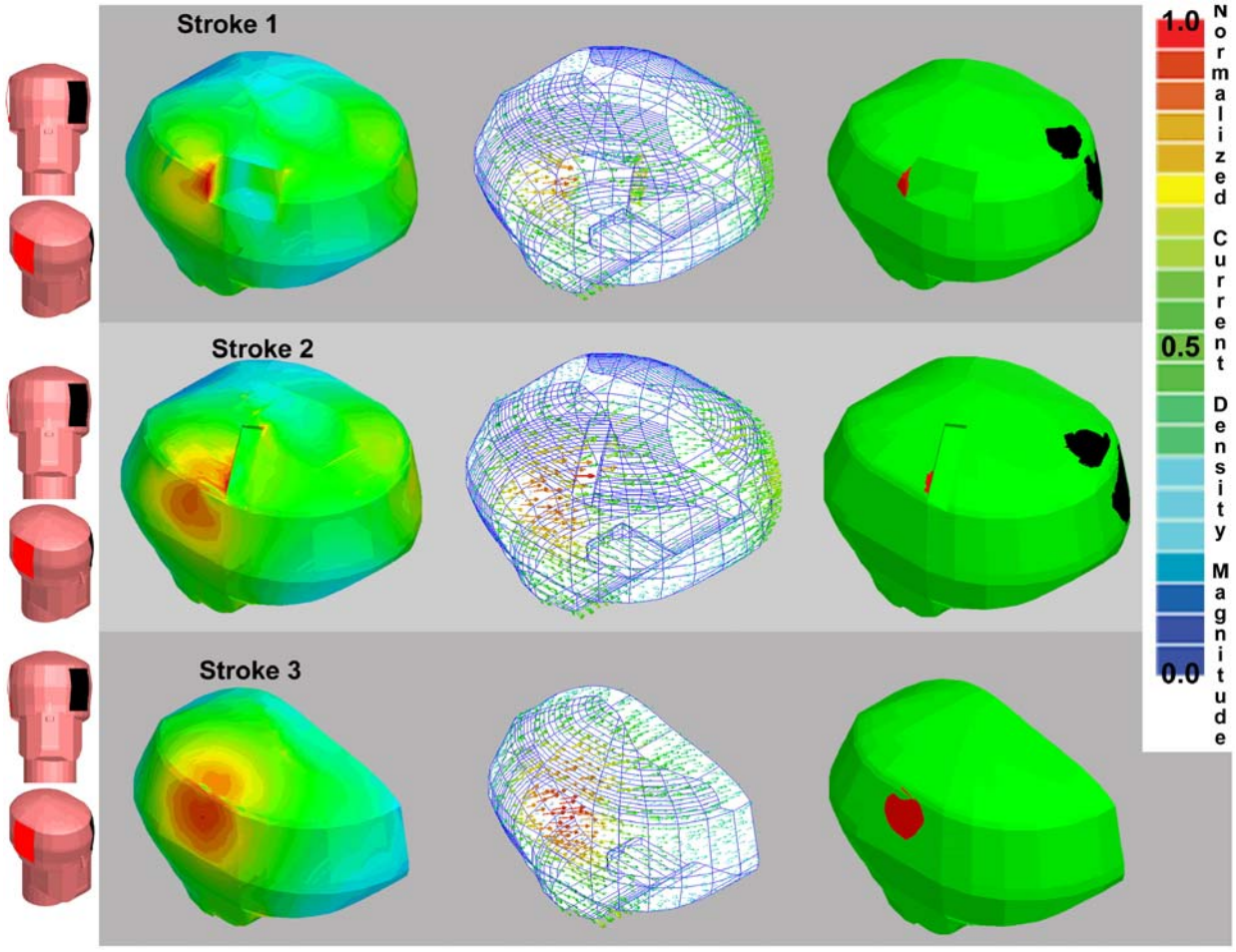

Fig. 6. Cortical current densities for Strokes 1–3. The layout is as explained in Fig. 2.

potential which is dependent upon the relative cortical neuron to current density orientations (Paulus, 2004).

Current density maxima

The change in the magnitude of the cortical current density maxima depended on the location and the area of the stimulating electrodes. The maximum cortical current density magnitudes are of the same order of magnitude of those cases recently published by Miranda et al. (2006). When the electrode sizes were varied the current density maxima decreased with increasing electrode size. Additionally, as the area of the electrodes decreased, the degree of shunting along the skin increased, indicative of an altered resistive matrix of the head system (i.e., the relative resistance of the tissues is dependent upon the electrode position and size and thus the overall resistance on which the current flows is dependent upon the electrode properties).

The location of the maxima was dependent on the electrode placement, which is indicative of the paths of current flow relative to the resistive matrix of the head. In general, the maximum cortical current density was greater when the electrodes were placed along scalp locations with less curvature of the head system, and when the curvature was maximized less current penetrated into the cortex and the shunting effect increased (for example if one looks at the 'anode over right M1–cathode over supra-orbital region' electrode montage they will notice that the current density is greater in the motor strip than in the supra-orbital region; where the overlying tissue layers are more planar with less curvature in the M1 region). This is to say that the resistive matrix was such that the current paths flowed more through the skin and the outer layers proximal to electrode locations along more curvilinear scalp locations. Based on this finding, one has to judge carefully the reliability of spherical models, which have been used as the basis for electrical stimulation modeling in the past (Saypol et al., 1991), as similar symmetry conditions have led to anomalous current density solutions while modeling other forms of brain stimulation (Wagner et al., 2004).

We have also shown that the cortical currents injected by 5×7 cm^2 and 5×5 cm^2 electrodes are similar (less than 5% difference), therefore use of one electrode type in lieu of the other might not have a significant clinical impact. In fact, the two clinical tDCS stroke studies used different electrodes size, 5×5 cm^2 (Hummel et al., 2005)and 5×7 cm^2 (Fregni et al., 2005b), and showed similar motor function improvement. Additionally, as we have shown that shunting effects increase with decreasing electrode area (see Montage1 vs. Montage 4), it is possible that some of the early discrepancies seen in the literature were simply related to unreported differences in electrode design. For example, compare the work of Bindman et al. (1964) to that of Arfai et al. (1970) and note that the inconsistent results appear to be obtained

with the same experimental design, however neither reports their electrode sizes.

Different electrode montages

The various electrode montages showed similar cortical current density magnitudes for all of the cases. The maximum cortical current density was found for the 'anode over V1–cathode over the vertex' electrode montage. In this case the electrodes were over a location on the cortex that was fairly flat and the electrodes were very close (less than 3.5 cm at shortest distance). However, it appears that the distance between the electrodes is less important than the overall relative location because we found the lowest cortical current density in the 'anode over the right DLPFC–cathode over the left DLPFC' electrode montage where the electrodes were also very close (less than 3.8 cm at shortest distance). In the case of the 'anode over the right M1–cathode over the left M1', the current density magnitudes in the cortex were actually larger than the case where the second electrode was placed over the contralateral supra-orbital region. This is again indicative of the resulting current density paths and the overall resistive matrix of the head tissue system.

Current density orientation

Since the 1960s it has been known that the orientation of the current densities is a key determinant in whether the cortex is facilitated or suppressed (i.e., whether the spontaneous activity is increased or decreased and whether the magnitudes of evoked potentials are greater or smaller following stimulation). Previous studies (Bindman et al., 1964; Landau et al., 1964; Purpura and McMurtry, 1965) showed that surface-positive cortical polarization (anode placement) excites the cortex and that the opposite effect is seen with surface negative polarization. Landau et al. (1964) showed that the surface effects could be reversed by placing the stimulating source within the cortex, such that the current density orientations were reversed relative to the stimulated neurons. In addition, Terzuolo and Bullock (1956) showed a similar effect in neural preparations. They observed that the change in the neural firing frequency with weak DC currents could be modulated based on the relative current to neural orientations. In more recent tDCS studies, Nitsche and Paulus (2000) showed that stimulation with the cathode placed above the motor cortex suppresses subsequent cortico-spinal responses, whereas facilitation of cortico-spinal responses is observed with the anode placed above the motor cortex. Additionally, behavioral task differences have been shown to be dependent on the use of anodal or cathodal tDCS over the same area. For instance, Fregni et al. (2005c) showed that anodal stimulation of the left dorsolateral prefrontal cortex leads to an enhancement of working memory that was not observed when the polarity was reversed. Similarly, while anodal stimulation of M1 or V5 increases significantly the percentage of correct tracking movements in the early learning phase, cathodal stimulation induces no significant effect on the performance of this task (Antal et al., 2004).

Thus, with the different electrode schemes studied, one can clearly see that changing the polarity of the electrodes is not the only way to alter the orientation of the injected current densities as varied anode and cathode positioning clearly alters the final current density orientations. For instance, when one compares the different current orientations (see Figs. 2 and 5) for the varied electrode positions it is apparent that changes in the position can have a drastic effect on the injected current orientations. And thus, it could be possible that multi-polar electrode schemes could be devised which could more accurately focus the currents in specific brain regions and future research based on this methodology should be explored.

Stroke model

Fields were altered in the stroke model, relative to the healthy head, such that the current density maxima were elevated and located directly along the stroke border for Stroke 1 and Stroke 2 and more inferior along the cortical surface for Stroke 3. The CSF in the infarction region provided a different conductive path for the currents away from the maximum current density location in the healthy head model. The kind of perturbations observed in the stroke models might occur with other pathologies. Therefore, in applying tDCS to abnormal patients, just as with other forms of brain stimulation (Wagner et al., 2006), it is critical to consider the location, geometry, and tissue characteristics of the pathological region, as adjustments of the stimulation montage might be needed to safely affect the desired cortical target. As we only report for 3 different models here, further research needs to be completed in this area. Additionally, we believe that the implications of the results should also be assessed when stimulation is applied in regions of major convolutions and gyri on the cortical surface as such inhomogeneities have been shown to alter the fields in other forms of stimulation (Miranda et al., 2003; Wagner et al., 2006).

Physics as a foundation for future studies

By exploring the current densities injected into the cortex during tDCS, this paper provides a foundation based on physics by which one can guide future clinical studies and explore fundamental aspects of this technique. In the healthy head model the magnitude of the cortical current density in the region of the cortex under a single electrode is primarily dependent on the scalp position of the electrode, the electrode size, the injected current density, and the relative electrical and anatomical properties of the tissues in the region. However, the current density orientations are dependent on the position of both electrodes. For example, if one compares Montage 2 with Montage 7, see Figs. 2 and 5, one will note that magnitude of the cortical current densities are not drastically different between the two montages (0.98 vs. 1.04 mA/cm^2 at the anode and 0.84 vs. 1.04 mA/cm^2 at the cathode respectively) but that the orientation of the current density vectors points in different directions. The cortical currents of Montage 2 are directed in a more dorsal to ventral orientation than the lateral to medial currents seen in Montage 7, see Figs. 2 and 5. This type of information provided by our modeling approach can guide future clinical studies. For example, clinical investigators could use the current density magnitude information to establish that induction of relatively selective changes in neural excitability in just one M1 could best be accomplished with Montage 2, or that Montage 7 is most likely to induce comparable changes in both the right and left M1s. Additionally a more pronounced effect in M1 could be achieved with Montage 7 than Montage 2 due to the increased cortical current density. From the general polarity of the currents, one would expect an overall inhibitory response under the cathode and a facilitatory response under the anode for both Montages 2 and 7, but one could

expect more subtle local changes based on the differences in the current density orientations. M1 is located under the anode in both montages, but the orientation of the currents in M1 depends on the cathode location and is thus different for each montage (see Figs. 2 and 5). In fact when one examines the study of Nitsche and Paulus (2000), they found that tDCS modulation of the cortical response of the abductor digiti minimi muscle was dependent on the relative electrode placement when comparing these two electrode montages (finding Montage 2 superior for modulation). As previously discussed, the relative current to axonal axis orientation is important in determining the degree of neural excitability changes, and thus with these two facts it is possible to expect that different neural populations would be affected unequally. Additionally, it should be noted that one would expect subtle differences dependent on individual anatomical variations (neural architecture and gross anatomical differences).

With the broad electrodes currently used in tDCS it is difficult to say how easy it will be for a clinician to harness these effects, but with future improvements in the technique such focal control might be possible. One could postulate the use of multiple electrodes of smaller dimensions and unequal current densities to influence neural populations based on their anatomical orientations relative to the calculated current densities. In the future, one could use the electromagnetic approach presented here to further increase the focality of tDCS without relying on complicated surgical procedures and studies and one could conceive of a clinical tracking system that predicts the current density distribution in patients relative to their individual MRIs and unique pathologies.

Clinical implications

Results of this study have several clinical implications and they can guide the design of future clinical studies using tDCS. First we will focus on major depression and stroke, where recent studies suggest a therapeutic potential of tDCS (Fregni et al., 2006a; Nitsche, 2002).

Several studies have shown that another noninvasive technique for brain stimulation (repetitive transcranial magnetic stimulation or rTMS) might be useful in the treatment of depression (see meta-analysis, Holtzheimer et al., 2001 or Couturier, 2005). The leading hypothesis to account for the antidepressant effects of rTMS (see review, Gershon et al., 2003) is that when high-frequency rTMS, which has been shown to increase cortical excitability, is applied to the left DLPFC it can normalize a pathological state of hypoactivity in depressed patients (or conversely low-frequency rTMS, which has been shown to decrease cortical excitability, to the right DLPFC can normalize the opposite hemisphere's state of hyperactivity) and stabilize an interhemispheric imbalance in activity thought to be causally related to the mood disturbance. The existing results would suggest that anodal tDCS of the left DLPFC or cathodal tDCS of the right DLPFC might both result in depression amelioration. Indeed, tDCS treatment using the electrode montage of anodal–left DLPFC and cathodal–contralateral supra-orbital (reference electrode) is associated with mood improvement in patients with treatment resistant depression (Fregni et al., 2006a). The results of our study show that this electrode montage with the supra-orbital reference, will result in adequate current magnitude in the area under the active electrode (i.e., the DLPFC electrode). An alternative approach would be the bilateral stimulation in which the excitability-enhancing anode electrode is placed over the left DLPFC and the excitability-diminishing cathode electrode is placed over the right DLPFC. Bilateral stimulation has been investigated before using rTMS (Hausmann et al., 2004), but due to technical limitations first one and then the other hemisphere were targeted. However, with the technique of tDCS, bilateral stimulation could be performed simultaneously, placing the anode and cathode over homologous regions of the right and left hemispheres. Our study shows that such a montage would lead to rather large shunting of currents given the proximity of both electrodes. Nevertheless, we show that the cortical current density in the DLPFC would be comparable for the "bilateral" montage when compared to the "unilateral" montage (anode on the DLPFC and cathode on the contralateral supra-orbital).

In stroke, recent research suggests that the facilitation of activity in the lesioned hemisphere and the suppression of activity in the undamaged hemisphere might both have a desirable therapeutic impact and promote recovery of function in these patients (Ward and Cohen, 2004). Given these aims, three tDCS approaches would seem to be reasonable: (1) anodal tDCS of the affected hemisphere with the expectation that activity will be increased; (2) cathodal tDCS of the unaffected hemisphere with the aim of reducing cortical excitability; and (3) bilateral stimulation in which both motor cortices are stimulated simultaneously by applying anodal tDCS to the affected and cathodal tDCS to the unaffected hemisphere. The results of our study show that the approaches (1) and (2) might induce significant and reliable currents in the cortex if the reference electrode is placed over the contralateral supra-orbital area. This finding is in accordance with recent clinical data (Fregni et al., 2005a; Hummel et al., 2005). Furthermore, our results show that bihemispheric stimulation will also induce currents in the motor cortices of adequate magnitude and thus may in fact allow for an even greater desirable modulation of bihemispheric activity and a larger behavioral effect size.

An important question when using tDCS in stroke is whether the stroke lesion would disturb the electric current similarly to what is observed in rTMS (Wagner et al., 2006). However, when one compares tDCS with rTMS in the case of stroke it is apparent that there are large differences in the degree of perturbation of the stimulating currents caused by the infarction depending on the stimulation methodology. We show that, differently from rTMS, the cortical current densities injected by tDCS in head models of stroke remain relatively unchanged. There certainly is a disturbance to the injected currents, with an increased current density at the location of the infarction border, but these remain in the range of magnitudes of stimulation in the healthy head model.

Our results should help the delineation of future clinical trials in other neuropathologies. For instance, we showed that the position of the electrode reference will not affect significantly the cortical current density magnitudes under the active electrode (see the '5×7 cm^2 right M1 anode–5×7 cm^2 contralateral lower neck cathode' montage). This might be particularly important for patients with epilepsy on whom the localization of the electrodes might need to vary according to the epileptogenic focus (see Fregni et al., 2006b). When one examines this '5×7 cm^2 right M1 anode–5×7 cm^2 contralateral lower neck cathode' montage it should be noted that negligible current densities were found in the brain stem region (most likely due to the neck electrode being placed on the contralateral ventral portion of the neck and the smaller area of the electrode contributing to shunting). However, one could clearly implement electrode montages that could influence brain stem activity, although this has been discouraged due to safety reasons (Nitsche et al., 2003).

Limitations and future improvements

Some limitations of this study suggest specific areas of possible future research. First, the resolution of the model is limited by the CAD rendering of the human head and does not share the same resolution as the MRI that was used to derive it. Additionally, further research needs to be completed on the DC tissue electrical properties to account for their anisotropies and heterogeneities. The model should be expanded in the future to account for these tissue properties as more data become available. Another limitation requiring further exploration comes from the fact that true stroke lesions have irregular borders and shapes that were not completely reproduced by our model. Work in this area should be pursued in the future.

Conclusions

This paper has presented models of the injected cortical current densities during tDCS. For the different electrode schemes studied, the calculated current density magnitudes are sufficient to conclude that in humans tDCS is indeed capable of altering ongoing cortical neural activity. Additionally, this study has demonstrated that tDCS effects are altered in the presence of cortical damage, though the effect is relatively small as compared with other brain stimulation techniques. The kind of perturbations observed in the stroke models will occur in other pathological cases in which the geometry or electrical characteristics of brain tissue are altered. We believe future studies focused on the effects of tissue anisotropies on the injected field, pathology effects on the injected fields, and the relative current orientation to the cellular micro-architecture should be pursued. Future efforts and model refinements will help optimize stimulation strategies for future clinical studies.

References

Akhtari, M., Bryant, H.C., Mamelak, A.N., Flynn, E.R., Heller, L., Shih, J.J., Mandelkern, M., Matlachov, A., Ranken, D.M., Best, E.D., et al., 2002. Conductivities of three-layer live human skull. Brain Topogr. 14 (3), 151–167.

Aldini, G., 1804. Essai theorique et experimental sur le galvanisme. Fournier, Paris.

Ansoft, 2005a. Asoft 3D Manual. Ansoft, Pittsburgh.

Ansoft, 2005b. Maxwell. Version 10 3D. Ansoft, Pittsburgh.

Antal, A., Kincses, T.Z., Nitsche, M.A., Paulus, W., 2003. Modulation of moving phosphene thresholds by transcranial direct current stimulation of V1 in human. Neuropsychologia 41 (13), 1802–1807.

Antal, A., Kincses, T.Z., Nitsche, M.A., Bartfai, O., Paulus, W., 2004. Excitability changes induced in the human primary visual cortex by transcranial direct current stimulation: direct electrophysiological evidence. Investig. Ophthalmol. Vis. Sci. 45 (2), 702–707.

Arfai, E., Theano, G., Montagu, J.D., Robin, A.A., 1970. A controlled study of polarization in depression. Br. J. Psychiatry 116 (533), 433–434.

Barker, A.T., 1994. Magnetic nerve stimulation: principles, advantages, and disadvantages. In: Ueno, S. (Ed.), Biomagnetic Stimulation. Plenum Press, New York.

Bindman, L.J., Lippold, O.C., Redfearn, J.W., 1964. The action of brief polarizing currents on the cerebral cortex of the rat (1) during current flow and (2) in the production of long-lasting after-effects. J. Physiol. 172, 369–382.

Bogdan, I., Zhou, P., 2004. 3D software levels of the electromagnetic field. Eng. Technol. 18–20.

Burger, H.C., Van Milaan, J.B., 1943. Measurement of the specific resistance of the human body to direct current. Acta Med. Scand. 114, 584–607.

Couturier, J.L., 2005. Efficacy of rapid-rate repetitive transcranial magnetic stimulation in the treatment of depression: a systematic review and meta-analysis. J. Psychiatry Neurosci. 30 (2), 83–90.

Crille, G.W., Hosmer, H.R., Rowland, A.F., 1922. The electrical conductivity of animal tissues under normal and pathological conditions. Am. J. Physiol. 60, 59–106.

De Mercato, G., Garcia Sanchez, F.J., 1992. Correlation between low-frequency electric conductivity and permittivity in the diaphysis of bovine femoral bone. IEEE Trans. Biomed. Eng. 39 (5), 523–526.

Foster, K.R., Schwan, H.P., 1996. Dielectric properties of tissues. In: Polk, C., Postow, E. (Eds.), Biological Effects of Electromagnetic Fields. CRC Press, New York, pp. 25–102.

Fregni, F., Boggio, P.S., Mansur, C.G., Wagner, T., Ferreira, M.J., Lima, M.C., Rigonatti, S.P., Marcolin, M.A., Freedman, S.D., Nitsche, M.A., et al., 2005a. Transcranial direct current stimulation of the unaffected hemisphere in stroke patients. NeuroReport 16 (14), 1551–1555.

Fregni, F., Boggio, P.S., Mansur, C.G., Wagner, T., Ferreira, M.J., Lima, M.C., Rigonatti, S.P., Marcolin, M.A., Freedman, S.D., Nitsche, M.A., et al., 2005b. Transcranial direct current stimulation of the unaffected hemisphere in stroke patients. NeuroReport 16 (14), 1551–1555.

Fregni, F., Boggio, P.S., Nitsche, M., Bermpohl, F., Antal, A., Feredoes, E., Marcolin, M.A., Rigonatti, S.P., Silva, M.T., Paulus, W., et al., 2005c. Anodal transcranial direct current stimulation of prefrontal cortex enhances working memory. Exp. Brain Res. 166 (1), 23–30.

Fregni, F., Boggio, P.S., Nitsche, M., Marcolin, M.A., Rigonatti, S.P., Pascual-Leone, A., 2006a. Treatment of major depression with transcranial direct current stimulation. Bipolar Disord 8 (2), 203–204.

Fregni, F., Thome-Souza, S., Nitsche, M., Freedman, S.D., Valente, K.D., Pascual, A.P, 2006b. A controlled clinical trial of cathodal DC polarization in patients with refractory epilepsy. Epilepsia 47 (2), 335–342.

Freygang, W.H., Landau, W.M., 1955. Some relations between resistivity and electrical activity in the cerebral cortex of the cat. J. Cell Comp. Physiol. 45, 377–392.

Gabriel, C., Gabriel, S. 1996. Compilation of the dielectric properties of body tissues at RF and microwave frequencies. San Antonio: Air Force Material Command, Brooks Air Force Base, TX. Report nr AL/OE-TR-1996-0037.

Geddes, L.A., 1987. Optimal stimulus duration for extracranial cortical stimulation. Neurosurgery 20 (1), 94–99.

Gershon, A.A., Dannon, P.N., Grunhaus, L., 2003. Transcranial magnetic stimulation in the treatment of depression. Am. J. Psychiatry 160 (5), 835–845.

Hall, K.M., Hicks, R.A., Hopkins, H.K., 1970. The effects of low level DC scalp positive and negative current on the performance of various tasks. Br. J. Psychiatry 117, 689–691.

Hasted, J.B., 1973. Aqueous Dielectrics. Halsted Press, New York. 302 pp.

Hausmann, A., Pascual-Leone, A., Kemmler, G., Rupp, C.I., Lechner-Schoner, T., Kramer-Reinstadler, K., Walpoth, M., Mechtcheriakov, S., Conca, A., Weiss, E.M., 2004. No deterioration of cognitive performance in an aggressive unilateral and bilateral antidepressant rTMS add-on trial. J. Clin. Psychiatry 65 (6), 772–782.

Holtzheimer III, P.E., Russo, J., Avery, D.H., 2001. A meta-analysis of repetitive transcranial magnetic stimulation in the treatment of depression. Psychopharmacol. Bull. 35 (4), 149–169.

Hummel, F., Celnik, P., Giraux, P., Floel, A., Wu, W.H., Gerloff, C., Cohen, L.G., 2005. Effects of non-invasive cortical stimulation on skilled motor function in chronic stroke. Brain 128 (Pt. 3), 490–499.

Iyer, M.B., Mattu, U., Grafman, J., Lomarev, M., Sato, S., Wassermann, E.M., 2005. Safety and cognitive effect of frontal DC brain polarization in healthy individuals. Neurology 64 (5), 872–875.

Jacobs, M.A., Zhang, Z.G., Knight, R.A., Soltanian-Zadeh, H., Goussev, A.V., Peck, D.J., Chopp, M., 2001. A model for multiparametric MRI tissue characterization in experimental cerebral ischemia with histological validation in rat. Part 1. Stroke 32 (4), 943–949.

Kim, Y., Webster, J.G., Tomkins, W.J., 1984. Simulated and experimental studies of temperature elevation around electrosurgical dispersive electrodes. IEEE Trans. Biomed. Eng. 31, 681–692.

Landau, W.M., Bishop, G.H., Clare, M.H., 1964. Analysis of the form and distribution of evoked cortical potentials under the influence of polarizing currents. J. Neurophysiol. 27, 788–813.

Lepeschkin, E., 1951. Modern Electrophysiology. Williams and Wilkins, Baltimore.

Lindemanns, F.W., Heethaar, R.M., Denier van der Gon, J.J., Zimmerman, A.N.E., 1975. Site of initial excitation and current threshold as a function of electrode radius in heart muscle. Cardiac. Res. 9, 95–104.

Lolas, F., 1976. Brain polarization: behavioral and therapeutic effects. Br. J. Psychiatry 12 (1), 1977.

Miranda, P.C., Hallett, M., Basser, P.J., 2003. The electric field induced in the brain by magnetic stimulation: a 3-D finite-element analysis of the effect of tissue heterogeneity and anisotropy. IEEE Trans. Biomed. Eng. 50 (9), 1074–1085.

Miranda, P.C., Lomarev, M., Hallett, M., 2006. Modeling the current distribution during transcranial direct current stimulation. Clin. Neurophysiol. 117 (7), 1623–1629.

Nathan, S.S., Sinha, S.R., Gordon, B., Lesser, R.P., Thakor, N.V., 1993. Determination of current density distributions generated by electrical stimulation of the human cerebral cortex. Electroencephalogr. Clin. Neurophysiol. 86 (3), 183–192.

Nitsche, M.A., 2002. Transcranial direct current stimulation: a new treatment for depression? Bipolar Disord. 4 (Suppl 1), 98–99.

Nitsche, M.A., Paulus, W., 2000. Excitability changes induced in the human motor cortex by weak transcranial direct current stimulation. J. Physiol. 527 (Pt 3), 633–639.

Nitsche, M.A., Paulus, W., 2001. Sustained excitability elevations induced by transcranial DC motor cortex stimulation in humans. Neurology 57 (10), 1899–1901.

Nitsche, M.A., Liebetanz, D., Tergau, F., Paulus, W., 2002. Modulation of cortical excitability by transcranial direct current stimulation. Nervenarzt 73 (4), 332–335.

Nitsche, M.A., Liebetanz, D., Lang, N., Antal, A., Tergau, F., Paulus, W., 2003. Safety criteria for transcranial direct current stimulation (tDCS) in humans. Clin. Neurophysiol. 114 (11), 2220–2222 (author reply 2222-3).

Nitsche, M.A., Grundey, J., Liebetanz, D., Lang, N., Tergau, F., Paulus, W., 2004a. Catecholaminergic consolidation of motor cortical neuroplasticity in humans. Cereb. Cortex 14 (11), 1240–1245.

Nitsche, M.A., Niehaus, L., Hoffmann, K.T., Hengst, S., Liebetanz, D., Paulus, W., Meyer, B.U., 2004b. MRI study of human brain exposed to weak direct current stimulation of the frontal cortex. Clin. Neurophysiol. 115 (10), 2419–2423.

Oswald, K., 1937. Messung der leitfahigkeit und Dielektrizitatkonstante biologischer Gewebe un Flussigkeiten bei kurzen Wellen. Hochfrequenztech. Elektroakust. 49, 40–49.

Paulus, W., 2004. Outlasting excitability shifts induced by direct current stimulation of the human brain. Suppl. Clin. Neurophysiol. 57, 708–714.

Priori, A., 2003. Brain polarization in humans: a reappraisal of an old tool for prolonged non-invasive modulation of brain excitability. Clin. Neurophysiol. 114 (4), 589–595.

Purpura, D.P., McMurtry, J.G., 1965. Intracellular activities and evoked potential changes during polarization of motor cortex. J. Neurophysiol. 28, 166–185.

Radvan-Ziemnowicz, J.C., McWilliams, J.C., Kucharski, W.E., 1964. In: Werner, Ma. (Ed.), Conductivity Versus Frequency in Human and Feline Cerebrospinal Fluid. Washington 12, DC.

Ranck, J.B., 1963. Specific impedance of rabbit cerebral cortex. Exp. Neurol. 7, 144–152.

Saypol, J.M., Roth, B.J., Cohen, L.G., Hallett, M., 1991. A theoretical comparison of electric and magnetic stimulation of the brain. Ann. Biomed. Eng. 19 (3), 317–328.

Sheffield, L.J., Mowbray, R.M., 1968. The effect of polarization on normal subjects. Br. J. Psychiatry 114, 225–232.

Soltanian-Zadeh, H., Pasnoor, M., Hammoud, R., Jacobs, M.A., Patel, S.C., Mitsias, P.D., Knight, R.A., Zheng, Z.G., Lu, M., Chopp, M., 2003. MRI tissue characterization of experimental cerebral ischemia in rat. J. Magn. Reson. Imaging 17 (4), 398–409.

Tehovnik, E.J., 1996. Electrical stimulation of neural tissue to evoke behavioral responses. J. Neurosci. Methods 65 (1), 1–17.

Terzuolo, C.A., Bullock, T.H., 1956. Measurement of imposed voltage gradient adequate to modulate neuronal firing. Proc. Natl. Acad. Sci. U. S. A. 42 (9), 687–694.

Wagner, T.A., Zahn, M., Grodzinsky, A.J., Pascual-Leone, A., 2004. Three-dimensional head model simulation of transcranial magnetic stimulation. IEEE Trans. Biomed. Eng. 51 (9), 1586–1598.

Wagner, T., Fregni, F., Eden, U., Ramos-Estebanez, C., Grodzinsky, A.J., Zahn, M., Pascual-Leone, A., 2006. Transcranial magnetic stimulation and stroke: a computer based human model study. NeuroImage 30 (3), 857–870.

Ward, N.S., Cohen, L.G., 2004. Mechanisms underlying recovery of motor function after stroke. Arch. Neurol. 61 (12), 1844–1848.